

# Bilateral Teleoperation of Flexible Surgical Robots

Mohsen Mahvash and Pierre Dupont

**Abstract**—We introduce a position-exchange controller for bilateral teleoperation of flexible surgical robots. The controller requires the position of the master arm and the deformed shape of the slave arm, but no force information is required. The position-tracking controller of the master arm causes the master arm to follow the position of the tip of the slave arm. The position tracking controller of the slave arm causes the slave to follow the position of the master and also deforms the shape of the slave arm until the force generated at its tip matches the force applied to the master. The position exchange controller is illustrated using two systems. The first is a simple one degree of freedom flexible robot. The second system is a surgical robot constructed from a set of precurved superelastic concentric tubes. The control structure enables fast computation of the deformed shape kinematics of the slave arm using Cosserat rod theory. Simulation results show that the controller provides transparency at the low frequencies necessary for palpation of soft tissue.

## I. INTRODUCTION

Robots for minimally invasive surgery have a small cross section and thus often flex during interaction with the surgical environment. This is true of snake-like surgical robots built from superelastic beams [1], [2], [3] as well as the slave manipulator of the da Vinci surgical system (Intuitive Surgical Inc.) [4], [5]. Link flexibility of the slave manipulator modifies its kinematic map and consequently reduces the transparency of the system in transmitting the environment stiffness to the user.

A position-tracking controller is often used for teleoperation of a surgical robot [6]. The position controller commands the surgical robot to follow the position of a master manipulator. Bilateral or force-feedback teleoperation is established by adding a position tracking controller to the master manipulator. The master position tracking controller applies force to the master when the slave is displaced from its goal position. The position-exchange controller does not require a force sensor to generate force feedback. However, it provides transparency at low frequencies for interaction with soft environments if the master and slave manipulators are rigid and the resistance dynamic of the robots are cancelled [6], [7].

For a flexible slave robot, a position-exchange controller transmits the series combination of the stiffness of the environment and the stiffness of the links of the robot. When the robot stiffness is less than the stiffness of the environment, the stiffness of the environment is not transmitted to the

user. This makes force feedback based on position exchange ineffective for palpation tasks [8] since the flexibility of slave does not allow the user to detect a hard spot on the surface of a soft object (for example, due to a tumor below the surface of a tissue).

We introduce a new position-exchange control strategy for bilateral teleoperation of a flexible surgical robot. The position controller of the master manipulator uses the difference between the tip positions of the master manipulator and the flexible slave robot to calculate the force that is applied to the master manipulator. The position controller of the slave manipulator deforms the slave manipulator to a desired shape that generates the master manipulator force at the tip of the slave manipulator. In steady state, when the manipulators do not move, the forces generated by master master manipulator and the slave manipulator match. The position error between the tip of the slave manipulator and the master manipulator is small and depends on the gain of the position tracking controllers. Thus, the controller provides transparency at low frequency.

Implementation of the slave position controller depends on the efficient solution of the inverse kinematics problem for the deformed manipulator. The solution presented here achieves efficiency by decomposing this problem into two steps. In the first step, a deformation model is used to compute the unloaded slave configuration that produces the desired tip force when in contact with the environment. Depending on the initial shape and the amount of deformation, the Cosserat rod model or the Euler-Bernoulli beam model can be used for this step. In the second step, the desired joint angles of the slave robot are computed from a kinematic model that assumes no forces are applied to the slave.

The first step of the slave position controller requires the shape of the slave manipulator. There are several different approaches available for measuring its shape. These include fiber optic shape sensors mounted inside or on the exterior of the arm [9], extracting the shape from real-time images of the slave robot and the use of electromagnetic trackers mounted at intervals along the manipulator to estimate its shape.

The remainder of the paper is organized as follows. To introduce the concepts, Section II explains the control law for bilateral teleoperation of a one degree of freedom flexible robot. Section III presents simulation results for this flexible robot illustrating the enhanced transparency and consequent improvement in transmitting environment stiffness for palpation. Section IV presents the controller for a concentric tube robot using a Cosserat rod model of deformation. Section V concludes the paper.

This work was supported by the National Institutes of Health under Grant R01 HL087797.

M. Mahvash and P. Dupont are with the Department of Aerospace and Mechanical Engineering, Boston University, Boston, 02215, USA, email pierre/mahvash@bu.edu

## II. TELEOPERATION OF A ONE DOF FLEXIBLE ROBOT

### A. Model

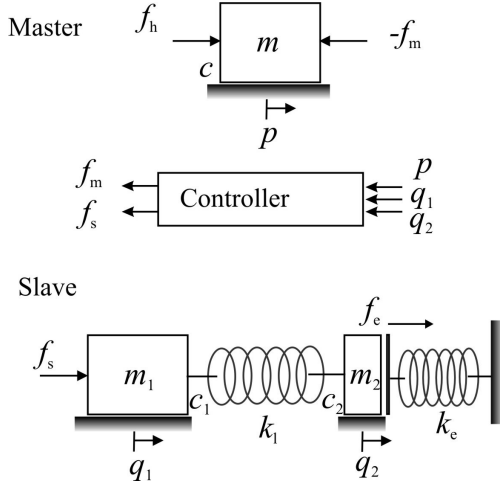


Fig. 1. The master arm, the position-exchange controller, and the flexible slave arm of a one DOF teleoperator

As shown in Figure 1, we assume the master manipulator is a one degree-of-freedom (DOF) rigid link and the slave manipulator is a one DOF elastic link. In order to clarify the analysis, we assume prismatic joints for the manipulators. The model for the flexible slave manipulator is written as:

$$\begin{aligned} m_1 \ddot{q}_1 + c_1 \dot{q}_1 &= -f_l + f_s \\ m_2 \ddot{q}_2 + c_2 \dot{q}_2 &= f_l + f_e \\ k_1(q_1 - q_2) &= f_l \end{aligned} \quad (1)$$

where  $q_1$  is the position of the actuator,  $q_2$  is the position of the tip,  $m_1$  is mass of the actuator,  $m_2$  is the mass of the tip (it is assumed the link inertia is concentrated at its tip),  $c_1$  and  $c_2$  are damping coefficients,  $f_l$  is the force transmitted through the elastic manipulator,  $k_1$  is the stiffness of the link,  $f_s$  is the generated force by the slave actuator, and  $f_e$  is the environment force.

The model for the master manipulator is written as (figure 1):

$$m \ddot{p} + c \dot{p} = f_m + f_h \quad (2)$$

where  $p$  is the position of the master tip,  $m$  and  $c$  are mass and damping values of the master manipulator respectively,  $f_m$  is the generated force by the master actuator and  $f_h$  is the operator force.

### B. Control Input

The position tracking controller for the master manipulator generates force  $f_m$  using a PD controller

$$f_m = -k_{c1}(p - q_2) - k_{c2}(\dot{p} - \dot{q}_2) \quad (3)$$

The goal of the slave manipulator controller is to apply this force  $f_m$  to the environment. To do so, it first calculates the desired actuator position,  $q_{d1}$ , and then employs a PD control

law to drive the actuator to this position. As described in the introduction, computation of the desired actuator position involves solving the inverse kinematics problem for the deformed slave manipulator. This proceeds in two steps.

- 1) Employ the deformation model to calculate the unloaded link configuration that produces the desired tip force, and
- 2) Solve the inverse kinematic problem for the joint variables that produce this configuration.

For this example, we need only address step one since, for a single prismatic joint, the kinematic map is trivial and the desired configuration corresponds to the desired joint variable,  $q_{d1}$ . The desired value is obtained from the link deformation (spring) model (last equation of (1)), the actual tip location of the deformed link ( $q_2$ ) and the master manipulator force,  $f_m$ .

$$q_{d1} = q_2 + \frac{f_m}{k_l} \quad (4)$$

The PD control law for input  $f_s$  is then calculated as

$$f_s = -k_{c3}(q_1 - q_{d1}) - k_{c4}(\dot{q}_1 - \dot{q}_{d1}) \quad (5)$$

### C. Transmitted Stiffness

To evaluate the capability of the proposed controller for palpation and to compare it to conventional position exchange control, we derive here the stiffness of the environment as transmitted to the operator by the controller (5). If the teleoperator transmits the actual environment stiffness,  $k_e$ , with small perturbations then the operator can distinguish changes of the environment stiffness during palpation [10], [8]. At steady state (figure 2), when the velocities and accelerations of the manipulators are zero, the models (1), (2), and the controller (5) reduce to

$$\begin{aligned} f_s &= f_l = k_l(q_1 - q_2) = -f_e = -k_e q_2 \\ f_h &= -f_m \\ f_s &= -k_{c3}(q_1 - q_{d1}) \end{aligned} \quad (6)$$

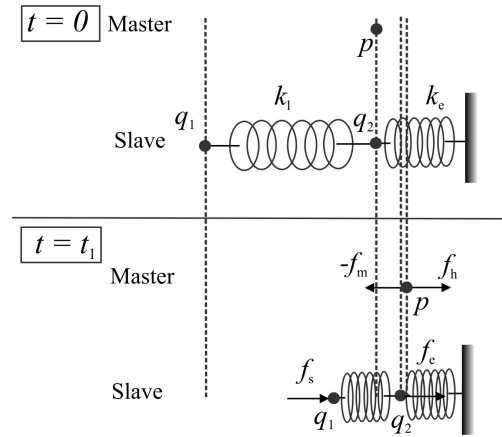


Fig. 2. Positions of the master and slave manipulators at the initial time  $t = 0$  and at steady state conditions,  $t = t_1$ .

These steady state conditions and (4) lead to

$$\begin{aligned} f_s &= -k_{c3}(q_1 - q_2 - \frac{f_m}{k_l}) = -k_{c3}(-\frac{f_e}{k_l} - \frac{f_m}{k_l}) \\ f_e &= k_{c3}(-\frac{f_e}{k_l} + \frac{f_h}{k_l}) \end{aligned} \quad (7)$$

Therefore

$$f_h = (1 + \frac{k_l}{k_{c3}})f_e \quad (8)$$

and full force transparency is obtained if  $k_{c3} \gg k_l$ . Considering (3), we conclude that in steady state

$$f_m = -k_{c1}(p - q_2) = -k_{c1}(p - \frac{f_e}{k_e}) \quad (9)$$

or

$$p = -\frac{f_m}{k_{c1}} + \frac{f_e}{k_e} \quad (10)$$

We divide (10) by  $f_h$

$$\frac{p}{f_h} = -\frac{f_m/f_h}{k_{c1}} + \frac{f_e/f_h}{k_e} \quad (11)$$

Given (8), we write

$$\frac{1}{k_t} = \frac{p}{f_h} = \frac{1}{k_{c1}} + \frac{1}{k_e(1 + \frac{k_l}{k_{c3}})}$$

where  $k_t$  is the transmitted stiffness to the operator. For high control gains  $k_{c1} \gg k_e$  and  $k_{c3} \gg k_l$ , the transmitted stiffness matches the environment stiffness.

If a conventional position exchange controller is used [8], it can be shown that the transmitted stiffness to the user is the series combination of the stiffnesses of the environment, the slave manipulator and the controller.

$$\frac{1}{k_t} = \frac{1}{k_{c1}} + \frac{1}{k_l} + \frac{1}{k_e}$$

For this controller, full transparency is not obtainable even for high control gains.

#### D. Stability

A conventional position-exchange controller uses only the position of the joints of the manipulators to calculate the joint torques of the manipulators. When the joint position sensors and the actuators of the manipulators are collocated, the torque-position mappings for the manipulators are passive. The position exchange controller implemented using PD controllers establishes a passive connection between the passive dynamics of the master manipulator and the slave manipulator and consequently the whole teleoperator (as a connection of three passive subsystems) is passive and remains stable when the teleoperator interacts with a passive environment and a passive operator.

In the case of non-collocated sensors and actuators, i.e., when the tip positions of a flexible slave manipulator are used as outputs for control, the input-output mapping for the manipulator can be active. In literature, modified tip positions such as the reflected tip position [11] and the

virtual angle of rotation [12] have been used to ensure a passive mapping for position trajectory control. An alternate approach has employed virtual time-variable dampers to make the position-trajectory controller of a flexible robot (using tip positions as outputs) passive [13]. One set of dampers were used at the joints of the flexible robot and another set at the port of a position trajectory generator for the slave manipulator. Here, we use constant joint dampers  $k_{c3}$  and a force-tracking damper  $k_{c4}$  to make the one DOF teleoperator passive for a linear passive load. The passivity condition for the teleoperator can be obtained using the absolute stability theorem [6].

### III. SIMULATION RESULTS

The telerobotic system of section II was simulated to evaluate its stiffness transparency and stability. For the simulation, the parameters of models (1) and (2) were selected as  $k_l = 200N/m$ ,  $c_1 = 3N/s$ ,  $c_2 = 0$ ,  $m_1 = 1kg$ ,  $m_2 = 0.1kg$ ,  $m = 0.5kg$ , and  $c = 3N/s$ . The controller parameters used were:  $k_{c1} = 5000N/s$ ,  $k_{c2} = 5000N/m$  and  $k_{c3} = k_{c4} = 300N/s$ .

A sinusoidal user force of  $f_h = 2\sin(\pi t)$  was used to probe an environment of stiffness  $k_e = 500N/m$ . Figure 3 compares the force-displacement response of the master manipulator to that of the environment. The close agreement indicates that the system could be used to differentiate changes in stiffness of the environment during palpation. The transmitted stiffness to the master manipulator is larger than the environment stiffness due to the force scale of (8). Figure 4 shows the force-displacement response of the master manipulator when conventional position exchange control is implemented with the same gains. As expected, the force-displacement response is more compliant than the flexible link and not at all representative of the environment stiffness.

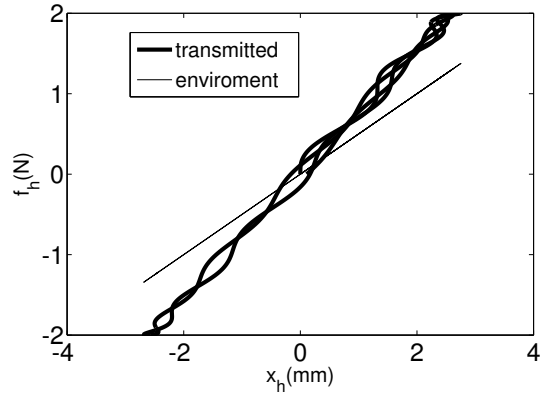


Fig. 3. Force-displacement of the operator and environment using the proposed controller

### IV. TELEOPERATION OF CONCENTRIC TUBE ROBOTS

In this section, the position-exchange controller of section II is applied to a teleoperator whose slave manipulator is

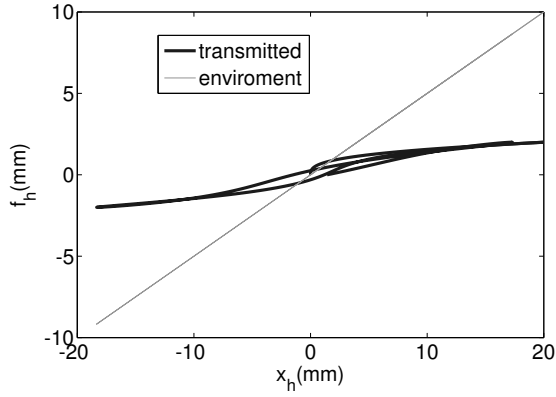


Fig. 4. Force-displacement of the operator and environment using the conventional position exchange controller

a concentric tube robot. A simple 5 DOF example is depicted in figure 5). With regard to controller implementation, there are two significant differences between the slave of the previous section and concentric tube robots. First, since concentric tube robots have substantial curvature along their length, a Cosserat rod model is needed to compute deformation due to environment forces. Secondly, since the shape of a concentric tube robot is determined by the relative rotations and translations of the precurved tubes that comprise it, its kinematics are nontrivial. The following subsection provides a brief introduction to concentric tube robots. This is followed by subsections that summarize the Cosserat rod and kinematic models needed for controller implementation. The controller is then described and simulated.

#### A. Concentric Tube Robot

Using the methodology proposed in [1], concentric tube robots are designed from a set of concentric superelastic tubes which are extended in telescoping fashion. Since they can be designed to have outer diameters of several millimeters, they are well suited for minimally invasive surgery. Since their curvature is controllable along their length, they are more versatile than traditional straight laparoscopic instruments. The authors are developing this technology for surgery inside the beating heart. For these applications, concentric tube robots are of comparable diameter to catheters, but are much stiffer. Consequently, they should enable higher fidelity position and force control for tissue interaction during surgery.

In the design approach proposed in [1], concentric tube robots are designed to be of piecewise constant curvature by combining in a telescoping fashion tube sections which are either of constant curvature or of variable curvature. A simple three-tube example is depicted in Figure 5. The outer pair of tubes proximal to the robot base form a variable curvature section while the portion of the innermost tube extending from the outer pair forms a constant curvature section. Constant curvature tubes are designed to be very

compliant in bending compared to the outer tubes of the concentric assembly. Thus, as seen in Figure 5, their retracted length conforms to the curvature of the outer tubes while their extended length conforms to their initial curvature.

As illustrated in Figure 6, a variable curvature section is comprised of two tubes of the same length and of similar bending stiffness. By appropriate choice of the initial tube curvatures, their combined curvature can be varied from zero to a maximum value by rotating the tubes with respect to each other. Thus, the kinematic variables for the three-tube 5 DOF design of Figure 5 consist of the extended arc lengths of the two sections and the rotation angles of the three tubes.

For clarity of exposition and without loss of generality, we consider here a concentric tube robot consisting of a single variable curvature section. This robot has 3 DOF for positioning its tip by varying its curvature, arc length and rotation angle through the kinematic variables of the two tube rotation angles,  $\theta_1$  and  $\theta_2$ , and their combined extension length,  $l$ .

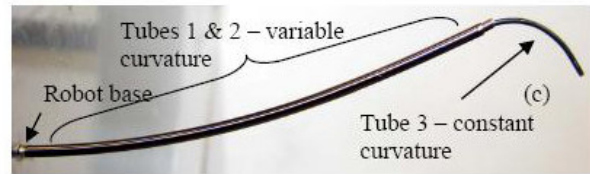


Fig. 5. 5 DOF concentric tube robot consists of two controllable sections.

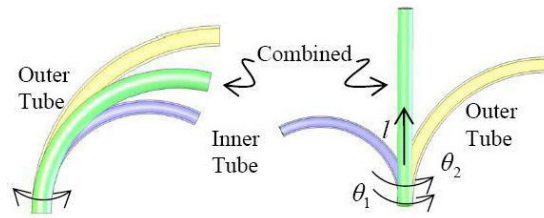


Fig. 6. Variable curvature section comprised of two concentric tubes of comparable bending stiffness. Curvature is varied by relative rotation of the tubes.

#### B. Kinematic Modeling

The kinematic model developed in [1], [14] is used here. To obtain a relatively simple algebraic kinematic model, the following assumptions are made:

- Each tubes initial curvature is piecewise constant.
- Tube bending is linear elastic.
- Torsional twist, cross sectional shear and longitudinal extension are negligible.
- The tubes experience pure bending (i.e., no transmitted forces)
- No external forces are applied.

The model results in a robot shape of piecewise constant curvature that has been shown to be relatively accurate for robots of moderate length [14].

For a robot comprised of a single variable curvature section, the tip position is calculated as a function of the tube joint variables,  $\{\theta_1, \theta_2, l\}$ . Coordinate frames are defined on each tube such that the  $z$  coordinate is tangent to the centerline of the tube and the curvature prior to assembly is entirely in the  $y$  coordinate direction,  $\bar{\kappa}_1 = [0 \ \bar{\kappa}_{1y} \ 0]^T$ ,  $\bar{\kappa}_2 = [0 \ \bar{\kappa}_{2y} \ 0]^T$ . The initial curvature vectors of the tubes must be transformed to the base frame of the robot by

$$\begin{aligned} \kappa_1 &= R(\theta_1)\bar{\kappa}_1 = [-\bar{\kappa}_{1y}\sin\theta_1 \ \bar{\kappa}_{1y}\cos\theta_1 \ 0]^T \\ \kappa_2 &= R(\theta_2)\bar{\kappa}_2 = [-\bar{\kappa}_{2y}\sin\theta_2 \ \bar{\kappa}_{2y}\cos\theta_2 \ 0]^T \end{aligned} \quad (12)$$

where  $R$  is a rotation matrix about the  $z$  axis.

The resultant curvature of the tube pair as function of  $\theta_1$  and  $\theta_2$  is obtained by writing the moment balance equation that holds for each point along the concentric tubes. Dropping the  $z$  component of curvature (always zero due to the assumption of torsional rigidity), the resultant curvature  $\kappa$  of tubes is obtained by [14]

$$\kappa_f = (K_1 + K_2)^{-1}(K_1\kappa_1 + K_2\kappa_2)$$

where  $K_i$  are diagonal stiffness matrices with diagonal elements equal to the bending stiffness  $E_i I_i$  of the cross section. Here,  $E_i$  is the modulus of elasticity and  $I_i$  is the cross sectional moment of inertia. The tip position  $q$  of the tube pair is then calculated by

$$q = \begin{bmatrix} \frac{\kappa_y(1 - \cos(l\|\kappa\|))}{\|\kappa\|^2} \\ -\frac{\kappa_x(1 - \cos(l\|\kappa\|))}{\|\kappa\|^2} \\ \frac{\sin(l\|\kappa\|)}{\|\kappa\|} \end{bmatrix} \quad (13)$$

A closed form solution for the inverse kinematics of the tube pair is obtained in [1] by combining (12) and (13). The reader is referred to this paper for the results.

### C. Cosserat Rod Model

To compute the deformation of a variable curvature tube pair due to an applied tip force, a Cosserat rod model is employed. In contrast with the kinematic model, the following assumptions are relaxed.

- A force is applied at the robot tip.
- The tubes can experience non-negligible twist, but do so as a pair.
- The tubes can transmit axial and shear forces along their length.

Given these assumptions, the tube pair is modeled as a single rod with a composite rotational stiffness matrix (bending and torsion)  $K$ ,

$$K = K_1 + K_2 \quad (14)$$

where  $K_i$  are diagonal  $3 \times 3$  stiffness matrices, with the first two diagonal components given by the bending stiffness as before and the third component describing torsional stiffness.

Following [15], the rod shape can be represented by a curve  $r(s)$  where  $s$  defines the arc length of the rod and  $r(s)$  is the position of the rod at  $s$  (figure 7). A coordinate frame

$E(s) = [e_1(s)e_2(s)e_3(s)r(s)]$  is defined at  $s$  such that its unit vector  $e_3(s)$  is tangent to  $r(s)$  and the frame rotates around  $e_3(s)$  when the rod experiences torsional twist. By defining the spatial velocity twist vector at each  $r(s)$  and evaluating it with respect to a collocated spatial frame, one obtains

$$\begin{bmatrix} v \\ u \end{bmatrix}^\wedge = \frac{dE}{ds}E^{-1} = \frac{dE}{ds} \quad (15)$$

where  $\wedge$  indicates the matrix form of the twist vector,  $v$  corresponds to the linear strain components and  $u$  to the rotational strain components of the rod. Due to the assumptions of negligible longitudinal and shear strain,  $v = [0 \ 0 \ 1]^T$ .

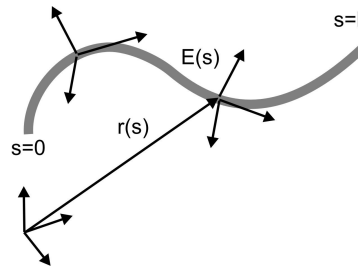


Fig. 7. Cosserat rod model

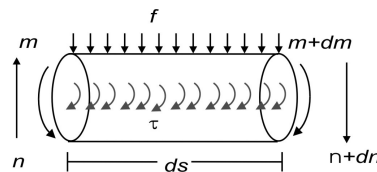


Fig. 8. Balance of force and moment for a differential length of rod

Taking into account that the coordinate frame is a function of  $s$ , the balance of moment and force for a length  $ds$  of the rod is written as (figure 8)

$$\begin{aligned} \frac{dm}{ds} &= \tau - [u]m - [v]n \\ \frac{dn}{ds} &= f - [u]n \end{aligned} \quad (16)$$

where  $m$  is transmitted cross sectional torque,  $n$  is transmitted cross sectional force,  $f$  is the applied force per unit length,  $\tau$  is applied torque per unit length and bracket notation on a vector indicates the associated skew symmetric matrix.

The constitutive law for rotational deformation of the rod is written

$$m = K(u - \hat{u}) \quad (17)$$

where, as before,  $K$  is the diagonal rotational stiffness matrix of the rod,  $u$  is the rotational strain (curvature) of the rod and  $\hat{u}$  is the strain (curvature) of the unloaded rod.

The boundary conditions for the rod are the location of its proximal end and the force applied at its tip (distal end),

$$\begin{aligned} E(s=0) &= E_0 \\ n(s=l) &= n_t \end{aligned} \quad (18)$$

where  $E_0$  the initial frame at the base of the beam and  $n_t$  is the applied tip force.

This set of boundary conditions does not produce a two-point boundary value problem. As described in [15], (16) can be efficiently integrated from the tip to the base yielding a set of local coordinate transformations along the rod. These transformations can then be concatenated with the base transform to locate the rods tip in base coordinates.

#### D. Position-Exchange Controller

To apply the position-exchange controller of section II to teleoperate a variable curvature concentric tube pair, the force  $f_s$  should be generated at its tip based on the current measured tip position of the master manipulator,  $p$ , and current tip position of the concentric tube pair,  $q$ ,

$$f_s = -K_{c1}(p - q) - K_{c2}(\dot{p} - \dot{q}) \quad (19)$$

where  $K_{c1}$  and  $K_{c2}$  are diagonal gain matrices.

To generate force  $f_s$ , the controller takes the current measured shape of the tubes,  $r_2(s)$ , as the shape of a Cosserat rod at rest and applies the force  $-f_s$  to it. The model of the previous subsection is used to compute the resulting rod shape  $r_1(s)$  and desired tip location,  $q_d$ , as shown in Figure 9. The algorithm requires  $\hat{u}$  which is assumed available from shape sensors. Note that  $r_1(s)$  is not necessarily of constant curvature. This is not a problem since it is the desired tip position,  $q_d$ , that is used as the input to the closed form inverse kinematic model to produce the associated joint variables,  $\theta_d$ . Finally, PD controllers are used to drive the joint variables to their desired values.

$$\tau_s = K_{c3}(\theta - \theta_d) + K_{c4}(\dot{\theta} - \dot{\theta}_d)$$

where  $\tau_s$  is the input torque to the actuators, and  $K_{c3}$  and  $K_{c4}$  are diagonal control gain matrices. In steady state,  $f_s$  converges to  $f_e$ .

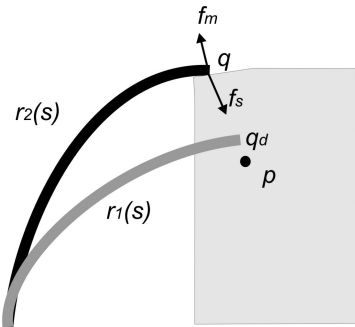


Fig. 9. Calculating the shape  $r_1(s)$  to produce the tip force.

When the concentric tube robot moves in free space,  $f_e = 0$ , and, as shown in figure 10, the difference between

the user position  $p$  and the robot tip  $q$  generates a small force  $f_s$ . Vector  $f_s$  is along the vector  $p - q$ . The controller calculates  $r_1(s)$  from the current tube shape  $r_2(s)$  defined by  $r_2(s)|_{t=t_0}$  and  $f_s$ . Due to force  $f_s$ , the tip of  $r_1(s)$  is moved toward  $p$ . The controller uses the tip location of  $r_1(s)$  to solve the inverse kinematic problem for the joint values that bring the concentric tube tip to the tip of  $r_1(s)$ . As the controller repeats this process, the position of the robot converges to the new user position.

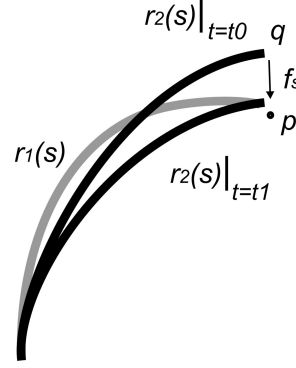


Fig. 10. Control algorithm for free space motion.

#### E. Simulation Result

We simulated the position-exchange control law for the 3 Dof concentric tube robot to study if the tip of the concentric tube robot follows the tip of the master manipulator and if the concentric tube converges to a desired configuration. For the simulation, the rotational stiffness of the tubes are selected as  $K = \text{diag}(300 \ 300 \ 300)$ , and no mass and damping are considered for the manipulators.

We simulated the free space motion of the concentric tube robot when the user suddenly moved the master manipulator from  $z = 42$  mm to  $z = 50$  mm. Figure 11 shows the tip displacement of the concentric tube robot along  $z$  and Figure 12 shows the shape trajectory of the concentric tube robot. The shape of the robot converges to a desired configuration when the displacement error between the master manipulator and the concentric tube robot converges to a small error.

## V. CONCLUSIONS AND FUTURE WORK

We presented a position-exchange control law for bilateral teleoperation of a flexible slave robot. The new control law provides complete transparency at zero frequency while conventional position-exchange control only does so when the manipulators are rigid. The control law was demonstrated in simulation for two systems. The latter example, comprised of concentric curved tubes, represents a complicated and yet practical application of the approach for surgical robots. Future work will include a stability analysis of the control law and relaxation of some assumptions of the kinematic and Cosserat models.

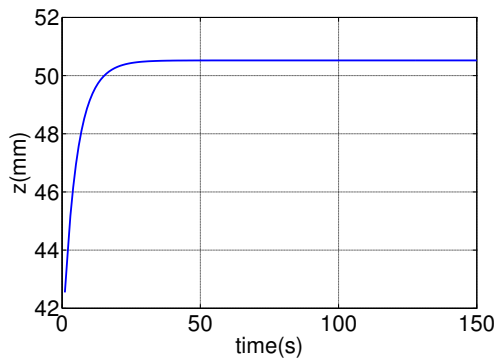


Fig. 11. Tip displacement of the concentric tube robot along  $z$  when the master manipulator is suddenly moved to  $z = 50\text{mm}$

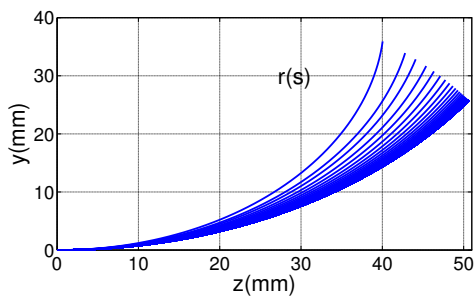


Fig. 12. The shape trajectory of the concentric tube robot when the tip of the robot is moved to a new location

## REFERENCES

- [1] P. Sears and P. Dupont, "A steerable needle technology using curved concentric tubes," in *IEEE/RSJ Int. Conference on Intelligent Robots and Systems*, Beijing, 2006, pp. 2850–2856.
- [2] R. J. Webster, A. M. Okamura, and N. J. Cowan, "Toward active cannulas: Miniature snake-like surgical robots," in *IEEE/RSJ Int. Conference on Intelligent Robots and Systems*, Beijing, 2006, pp. 2857–2863.
- [3] N. Simaan, R. Taylor, and P. Flint, "A dexterous system for laryngeal surgery," in *Proc. IEEE Intl. Conf. on Robotics and Automation*, New Orleans, April 2004, pp. 351–357.
- [4] G. S. Guthart and J. K., "The Intuitive telesurgery system: Overview and application," in *Proc. IEEE Int. Conf. Robotics and Automation*, San Francisco, CA, April 2000, pp. 618–621.
- [5] [Http://www.intuitivesurgical.com/](http://www.intuitivesurgical.com/).
- [6] M. Mahvash and A. Okamura, "Enhancing transparency of a position-exchange teleoperator," in *WorldHaptics Conference*, 2007, pp. 470–475.
- [7] D. A. Lawrence, "Stability and transparency in bilateral teleoperation," *IEEE Transactions on Robotics and Automation*, vol. 9, no. 5, pp. 624–637, 1993.
- [8] M. Mahvash, J. Gwilliam, R. Agarwal, B. Vagvolgyi, L. Su, D. Yuh, and A. Okamura, "Force feedback surgical teleoperator: controller design and palpation experiments," in *Symposium on Haptic Interfaces for Virtual Environments and Teleoperator Systems*, 2008, p. In press.
- [9] [Http://www.lunainnovations.com/](http://www.lunainnovations.com/).
- [10] L. A. Jones and I. W. Hunter, "A perceptual analysis of stiffness," *Experimental Brain Research*, no. 79, pp. 150–156, 1990.
- [11] D. Wang and M. Vidyasagar, "Passivity control of a single flexible link," in *IEEE Int. Conference on Robotics and Automation*, 1990, pp. 1432–1437.
- [12] P. A. Chodavarapu and M. W. Spong, "On noncollocated control of a single flexible link," in *IEEE Int. Conference on Robotics and Automation*, Minneapolis, MN, April 1996, pp. 1101–1106.
- [13] J. Ryu, D. Kwon, and B. Hannaford, "Control of a flexible manipulator with noncollocated feedback: Time domain passivity approach," *IEEE Transactions on Robotics*, vol. 20, no. 4, pp. 776–780, 2004.
- [14] P. Sears and P. Dupont, "Inverse kinematics of concentric tube steerable needles," in *IEEE Int. Conference on Robotics and Automation*, Rome, Italy, 2007, pp. 1887–1892.
- [15] D. Pai, "Strands: Interactive simulation of thin solids using cosserat models," in *Proceedings of Eurographics'02*, vol. 21, no. 3, 1990, pp. 347–352.